SAND2015-3953C
SAE 2015-01-1804

Detailed Characterization of Negative Valve Overlap Chemistry by Photoionization Mass Spectroscopy

Isaac W. Ekoto, Scott A. Skeen, Richard R. Steeper, Nils P. Hansen
Sandia National Laboratories

Abstract

For next-generation engines that operate using low-temperature gasoline combustion (LTGC) modes, a major issue remains poor combustion stability at low-loads. Negative valve overlap (NVO) enables enhanced main combustion control through modified valve timings to retain combustion residuals along with a small fuel injection that partially reacts during the recompression. While the thermal effects of NVO fueling on main combustion are well understood, the chemical effects of NVO reactions are less certain, especially oxygen-deficient reactions where fuel pyrolysis dominates. To better understand NVO period chemistry details, comprehensive speciation of engine samples collected at the end of the NVO cycle was performed by photoionization mass spectroscopy (PIMS) using synchrotron generated vacuum-ultraviolet light. Two operating conditions were explored: 1) a fuel lean condition with a short NVO fuel injection and a relatively high amount of excess oxygen in the NVO cycle (7%), and 2) a fuel-rich condition with a longer NVO fuel injection and low amount of NVO-cycle excess oxygen (4%). Samples were collected by a custom dump-valve apparatus from a direct injection, single-cylinder, automotive research engine operating under low-load LTGC and fueled by either isooctane or an 88-octane research certification gasoline. Samples were stored in heated stainless steel cylinders and transported to the Lawrence Berkeley National Laboratory Advanced Light Source for analysis using a Sandia National Laboratories flame sampling apparatus.

For all isooctane fueled conditions, NVO cycle sample speciation from the PIMS measurements agreed well with previously reported GC sample measurements if the sum total of all isomer constituents from the PIMS measurements were considered. PIMS data, however, provides richer speciation information that is useful for validation of computational modeling approaches. The PIMS data also revealed that certain species for the GC diagnostic were either misidentified during the calibration process or not identified at all. Examples of unidentified species include several classes of oxygenates (e.g., ketenes, aldehydes, and simple alcohols) and simple aromatics (e.g., benzene and toluene). For the gasoline fueled NVO cycles, performance characteristics were well matched to corresponding isooctane fueled NVO cycles. However, significant PIMS cross-talk from a wide range of gasoline components restricted the sampling analysis to a handful of species. Nonetheless, it was confirmed that for fuel-lean NVO operation there was a comparable increase in acetylene with NVO injection timing retard that is attributed to the prevalence of locally-rich, piston-surface pool fires caused by fuel spray impingement.

Introduction

The relentless drive for clean and efficient automotive engines has motivated research in low-temperature gasoline combustion (LTGC) strategies [1, 2]. Next-generation LTGC engines can achieve excellent fuel economy while still meeting ultra-low emissions standards. For LTGC, compression-induced auto-ignition is used to avoid high flame temperatures that result in nitrogen oxide formation typically associated with spark ignition. However, auto-ignition control is a challenge, especially at low specific engine output power operating points when mixture compositions are highly dilute and charge temperatures are low [3, 4].

The negative valve overlap (NVO) strategy has been used to overcome the low-load challenge via retained cylinder-combustion products in a recompression stroke along with a small injection of fuel [4, 5]. The subsequent main-cycle combustion stability is enhanced through a combination of charge heat addition from retained exhaust energy and NVO-period fuel oxidation [3, 5-22], along with enhanced mixture reactivity from partial fuel reformation [3, 10-12, 17, 22-24]. Despite extensive research characterizing products of NVO fueling via laser diagnostics [25, 26] and, more recently, using direct engine sampling [22, 24, 27], much remains uncertain about NVO chemistry.

Detailed end-cycle NVO speciation is needed to improve the fundamental understanding of the dominant chemical effects. Species characterization during NVO is complicated by the fact that intermediates are retained and consumed during the subsequent main combustion cycle. Laser-based absorption and fluorescence diagnostics enable spatially and/or temporally resolved measurements of charge temperature and number density for select species [14, 16, 18, 26, 28, 29], but are generally insufficient for comprehensive mixture speciation. Direct sampling with follow-on analysis by either gas chromatography (GC) or Fourier transform infrared spectroscopy (FTIR) diagnostics has provided important speciation details at the start and end of the NVO cycle [22, 24, 27, 30-32]. These methods hinge on the application of suitable gas-sampling systems that are free of biases from quenching or mixture stratification.

It was observed during previous sampling studies that the products of rich combustion (e.g., acetylene and ethylene) increased for a

globally lean NVO operation point as the NVO start of injection (SOI) was retarded [22]. The increase was attributed to pyrolysis reactions from piston surface pool fires as fuel spray impingement increased [17]. Conversely, these same rich products were observed with NVO SOI advanced for a globally rich operating point, which was thought to be from increased residence time for overly rich bulk-gas reactions [24, 27]. Sampling measurements have provided valuable data, although information supplied by the GC and FTIR diagnostics has so far been incomplete. The GC flame ion detector (FID) is not sensitive to aldehydes and cannot distinguish hydrocarbon isomers due to identical elution times. FTIR measurements on the other hand have been inconclusive due to large amounts of channel cross-talk that is difficult to account for during calibration. Accordingly, attempts to model NVO-cycle chemistry effects have largely been inconclusive due to a lack of complete speciation data [10, 12, 17, 33].

To overcome previous diagnostic difficulties, comprehensive species characterization of collected samples was performed via photoionization mass spectroscopy (PIMS) using vacuum-ultraviolet (VUV) light. Experiments were carried out using a Sandia-developed flame-sampling apparatus located at the Lawrence Berkeley National Laboratory Advanced Light Source (LNBL ALS) [34]. Multiple samples from a sweep of NVO fuel injection timings for a low and high excess oxygen NVO condition were collected at Sandia National Laboratories into heated stainless steel sample bottles. Samples were diluted by argon and transported to the ALS where they were analyzed using a predefined protocol.

The goal of the current study was to perform detailed speciation of engine samples collected at the end of the NVO cycle using PIMS. These data are then used to (1) provide validation measurements for NVO-cycle combustion modeling, (2) elucidate dominant constituents responsible for enhanced main combustion phenomena, and (3) provide calibration information for a complementary in-house GC diagnostic.

Approach

Engine

An optically accessible single-cylinder research engine configured for LTGC operation was used, with all-metal components replacing quartz windows for the current experiments. The flat-top piston from the optical configuration has been preserved. The pent-roof cylinder head contains one exhaust and two intake valves along with a centrally mounted, vertically oriented, 8-hole direct injector (see Figure 1). Exhaust valve closing (EVC) and intake valve opening (IVO) occurred 75 crank angle degrees (CAD) before and after NVO top dead center (TDC_{NVO}) respectively, with roughly 50% of the residual exhaust gases retained. NVO samples were collected using a custom dump-valve apparatus previously described in detail by Steeper and Davisson as well as by Peterson et al. [22]. The dump-valve assembly has direct access into the cylinder through one of two spark plug ports, with the other port used to house an embedded thermocouple so that head surface temperature can be continuously monitored.

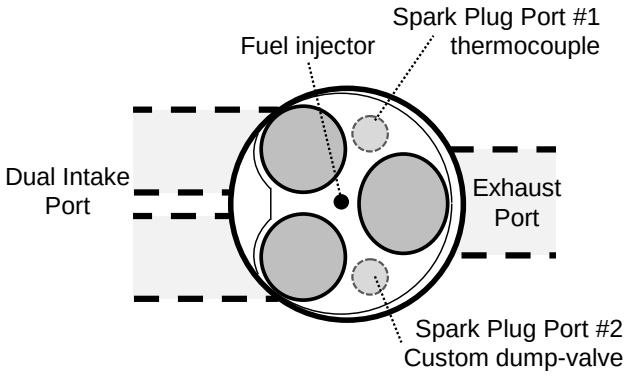

Figure 1: Schematic of the pent-roof cylinder head valve, spark plug, and injector arrangement.

To simplify sample gas speciation and facilitate future NVO-cycle modeling, isooctane was selected as a gasoline surrogate. For comparison, sampling and performance data were also acquired from the engine fueled by an 88-octane research gasoline (RD587) that contained 10% ethanol by volume for the globally lean NVO operating condition. Characteristics for the research gasoline are summarized in Table 1. Fuel injection rates for both the NVO and main cycles were set using custom injection timings from a predefined calibration map. Total fuel injection rate was monitored using a Max Machinery Model 213 flow meter. While the NVO fueling rate was fixed for both fuels, the main fueling rate for the RD587 gasoline was adjusted such that the total fuel energy injected was matched. The overall difference in fueling rates for the respective fuels was minor since the increased density of the reference gasoline was mostly offset by the larger isooctane heating value.

Table 1. Specifications for the reference isooctane and RD587 research fuels.

Distillation Temperature(s) [K] Isooctane RD587 (10%, 50%, 90%)	 372.1 330.5, 371.4, 429.3
Isooctane Element [Wt%]	Carbon: 84.12% Hydrogen: 15.88%
RD587 Element [Wt%]	Carbon: 82.67% Hydrogen: 13.68% Oxygen: 3.65%
RD587 Composition [Vol%]	Ethanol: 9.9% Saturates: 66.5% Olefins: 4.7% Aromatics: 18.9%
Heat of Combustion [MJ/kg] Isooctane RD587	 44.31 41.87
Density @ 15.56°C [g/mL] Isooctane RD587	 0.692 0.748
Octane Number (RON + MON)/2 Isooctane RD587	 100 88.4

Two operating conditions were explored: (1) a globally lean NVO operating point with elevated excess oxygen (7%) and a small NVO fuel injection (1.3 mg/inj.), and (2) a globally rich NVO operating point with little excess oxygen (4%) and a comparatively larger NVO fuel injection (6.0 mg/inj.). For both conditions, the intake air pressure was fixed at 100 kPa and the engine speed was kept a constant 1200 rpm. The intake air temperature was increased from

88°C for the globally rich NVO condition to 120°C for the globally lean NVO condition so that good combustion stability was maintained (~3% coefficient of variation). The NVO-cycle SOI was swept from shortly after EVC until at or just past NVO top dead center (TDC_{NVO}). Engine specifications and operating conditions along with NVO-cycle fueling rates and bulk-averaged equivalence ratios for each condition are listed in Table 2.

Table 2. Engine Specifications and Operating Conditions.

Displaced volume [liter]	0.633
Stroke [mm]	95.25
Bore [mm]	92
Compression ratio	11.3:1
Number of Valves	3 (2 intake, 1 exhaust)
Inlet Valve Open & Close	+75 CAD_{NVO} & -140 CAD_{MAIN}
Exhaust Valve Open & Close, EVO	+140 CAD_{MAIN} & -75 CAD_{NVO}
Residual Gas Fraction	0.50
NVO Duration [CAD]	150
Valve Lift [mm]	3
Speed [rpm]	1200
Intake Air Pressure [kPa]	100
Fuel Pressure [bar]	100
Exhaust Excess O_2 [%]	7 & 4
Intake Temperature [°C] 7% Exhaust Excess O_2 4% Exhaust Excess O_2	 88 120
Main Fueling Rate [mg/inj.] 7% Exhaust Excess O_2 4% Exhaust Excess O_2	Isooctane/**RD587** 8.3/**8.1** 9.9/**N/A**
Main SOI [CAD_{MAIN}]	-270
NVO Fueling Rate [mg/inj] 7% Exhaust Excess O_2 4% Exhaust Excess O_2	 1.3 6.0
NVO Global Equivalence Ratio 7% Exhaust Excess O_2 4% Exhaust Excess O_2	 0.45 2.13
NVO SOI (CAD_{NVO}) 7% Exhaust Excess O_2 4% Exhaust Excess O_2	 -55, -30, -20, -10, -5 -40, -10, 10

Gas-Sampling

The 8-mm dump-valve head diameter was designed to fit into the 14-mm threaded spark-plug port described earlier, and has a valve lift of 3.2 mm. A vacuum evacuated sample manifold connected the dump valve to a 1-liter, Teflon-lined, stainless steel sample bottle (see the illustration in Figure 2). All sample system components were insulated and kept at a constant 90°C by electric tape heaters connected to PID controllers to avoid water and hydrocarbon condensation. Exhaust stream gas sampling was also performed to measure the change in EVC input constituents.

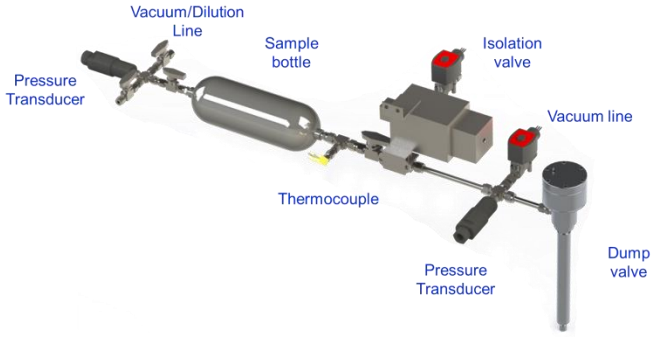

Figure 2: Illustration of the custom dump valve system and sample bottle.

During engine warm-up, port-fueled DME injections were used to quickly heat cylinder surfaces to 120°C. The DME injections were then replaced by direct isooctane or RD587 injections, with the total fueling rate set to achieve the desired exhaust O_2 concentration. Once cylinder wall temperatures reached 127°C, the dump-valve cycle sequence was activated (illustrated in Figure 3). The sequence began with a dump-cycle that featured a custom NVO injection rate, no main injection, and activation of the dump-valve system. The dump-cycle was then followed by continuous motored cycles. During the dump-cycle, dump-valve actuation began at -200 CAD_{MAIN} and continued until just after main-cycle TDC as a mix of NVO-cycle gasses plus fresh intake air collected in the sample bottle.

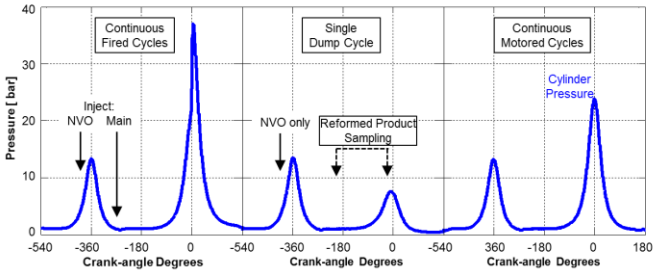

Figure 3: Schematic of the dump-valve cycle-sequence. Note that injection timings are reported with respect to the dump-cycle NVO TDC.

To estimate NVO species concentrations prior to IVO, the effect of sample dilution by the freshly mixed intake charge was compensated during post-processing. Note that Peterson et al. [24] compared GC speciation of engine exhaust samples with NVO samples without NVO fuel injection, and concluded the sampling system does not significantly impact intake breathing. Dump-sampling was repeated until the bottle pressure slightly exceeded atmospheric pressure. At this point, the engine was stopped with the sample bottle isolated and the bottle temperature and pressure recorded. The sample bottle was filled with pure argon until the bottle pressure reached roughly 3 bar. Sample bottle pressure and temperature were again recorded so that the amount of added dilution argon could be determined.

Two chromatograms created from an analysis of engine sample by in-house GC are presented in Figure 4, with known peaks from single-point calibrations identified. From the FID#1 column used to identify large hydrocarbon intermediates, it is apparent that numerous large hydrocarbon species that may be soot precursors have not been identified. From the FID#2 column, small concentrations of smaller hydrocarbon intermediates remain unidentified. Furthermore, it remains unclear if the calibrated species have been misidentified.

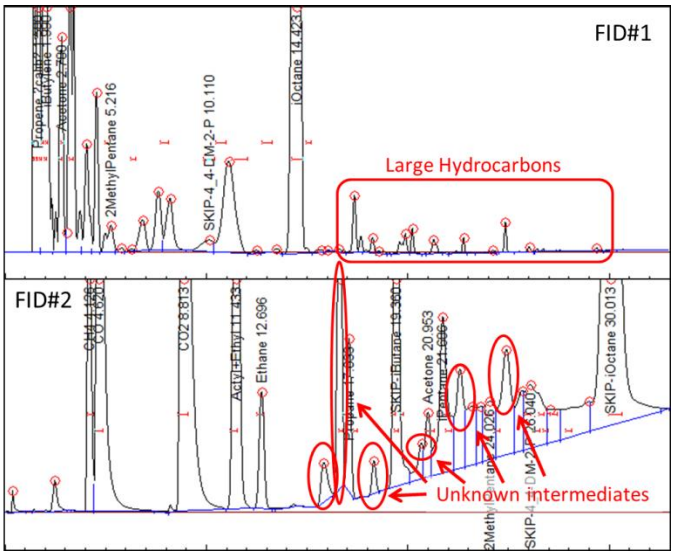

Figure 4: Sample chromatograms from the two FID detectors during a typical sampling run. Several intermediate species remain unidentified, including numerous hydrocarbons larger than the parent isooctane fuel.

Samples were transported to the LBNL ALS to be analyzed using a flame sampling apparatus owned and operated by Sandia's Combustion Chemistry department. Key details of the sampling apparatus are described below. Every effort was made to minimize the time between sample collection at Sandia and sample characterization at the ALS. Fresh samples were produced in the Sandia engine using the protocol described above, and then transported to the ALS (~1 hour drive). The largest time lag between sample generation and characterization was ~4 hours. Even for fresh samples, there was no chance to capture and identify short-lived intermediates. However, many of these species were likely quenched by the NVO-cycle expansion, with the surviving intermediates expected to be metastable. To investigate if species composition was impacted by long time delays, 4 samples at select operating points were intentionally generated 24 hours before characterization. No significant variation was observed.

Flame Sampling Apparatus Description

Detailed characterization of collected engine samples was performed using a Sandia owned flame-sampling apparatus originally designed for *ex situ* flame species measurements. A brief discussion is presented here, but the reader is referred to Cool et al. [34] for more details about the apparatus and Hansen et al. [35] for details about the PIMS diagnostic. Within the flame chamber, samples were expanded to a pressure of ~10^{-4} Torr through a quartz nozzle. The effusive flow was further expanded through a nickel skimmer to a pressure of ~10^{-6} Torr to create the desired molecular beam. Tunable VUV light from the LBNL ALS Chemical Dynamics beamline was used to continuously ionize the molecular beam in the extraction region of a high-resolution, reflectron, time-of-flight mass spectrometer. Ions were extracted into a flight tube at a 30 kHz repetition rate and with mass spectra up 250 atomic mass units (AMU) detected on a multichannel plate detector.

The low-pressure flame chamber was modified to accept direct input from the heated sample cylinders. Samples were metered into the flame chamber by an MKS 1179 flow controller at a low flow rate (85 cc/min) to maximize the sampling duration and hence the collected signal. A PID controller connected to the bottle heat tape with temperature feedback from an embedded thermocouple was used to keep sample bottle temperatures warm (~50°C). Engine sample speciation was accomplished by scanning across a range of relevant the photon energies (9.7–12.3 eV in 0.05 eV increments). An energy scan was also performed on a calibration bottle that contained 1000 ppm each of 8 hydrocarbons with a range of molecular weights (methane, acetylene, ethylene, propene, 1-butene, cyclopentene, benzene, and toluene).

PIMS Signal Post-Processing

For each energy scan, background noise was subtracted from the ion count signal, with wavelet filters applied for further noise reduction. Signal time-of-flight measurements were correlated to the ion mass by a predefined calibration, with the signal counts binned in 1 AMU units to maximize signal-to-noise (SNR) and facilitate spectral analysis. Processed signal from each energy scan was then stitched together to form an energy scan image as a function of photon energy and AMU. An example is provided in the top image in Figure 5.

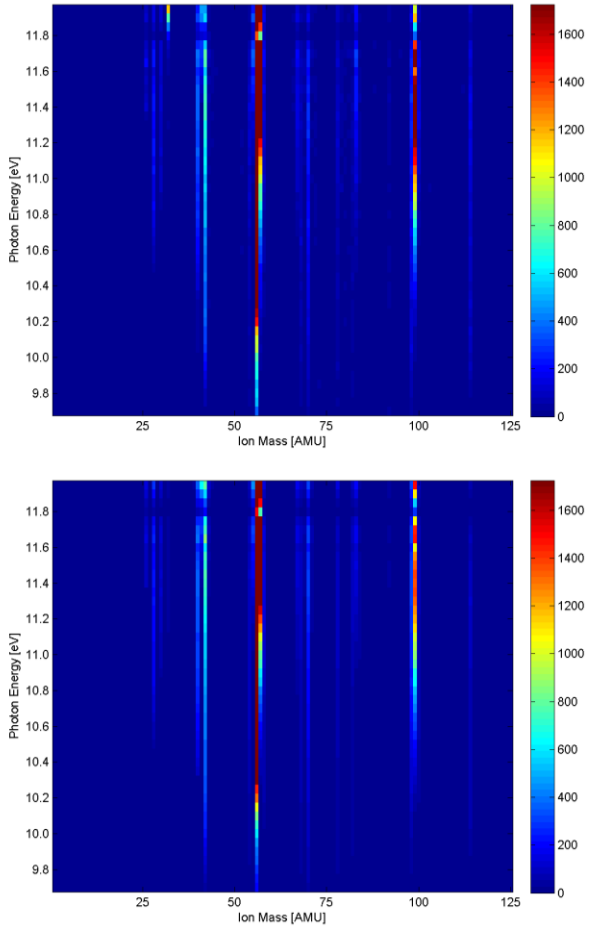

Figure 5. Raw energy scan image for the globally rich NVO operating condition (SOI = -40 CAD_{NVO}) engine sample (top) and corresponding synthetic energy scan image with optimized species concentrations (bottom).

A custom algorithm was developed to determine species constituents from the each energy scan image. Signal post-processing was simplified from the method described by Cool et al. [34], to reflect the fact that the metered engine samples were isothermal.

Accordingly, the ion count S for mass i at energy E is related to the species mole fraction χ as:

1. $$S_i(E) = \chi_i \cdot \sigma_i(E) \cdot D_i \cdot \Phi(E) \cdot PD_{eff}(E) \cdot SW(E) \cdot C(E)$$

Here, σ is the photoionization cross-section (PICS), D is a mass discrimination factor that depends on mass spectrometer ion focusing, Φ is the photon flux, and PD_{eff} is the corresponding photodetector efficiency. Note that photo-dissociation processes can result in the formation of smaller ion fragments, which accordingly result in multiple photoionization terms for each energy level. Comprehensive photoionization cross-section libraries for 335 hydrocarbon species, oxidants, diluents, and flame intermediates across a range of energies were consolidated from several sources. For cross-section libraries missing data at higher energies (i.e., up to 12.3 eV), these values were estimated from linear extrapolation of lower energy values. Extrapolated libraries were found to agree well with the calibration datasets, but nonetheless introduced additional uncertainty during post-processing. An example of the reference and extrapolated libraries for cis-2-butene and isooctane are provided in Figure 6. Note that signal from the parent isooctane ion is negligible, with species determination primarily from its fragment ions.

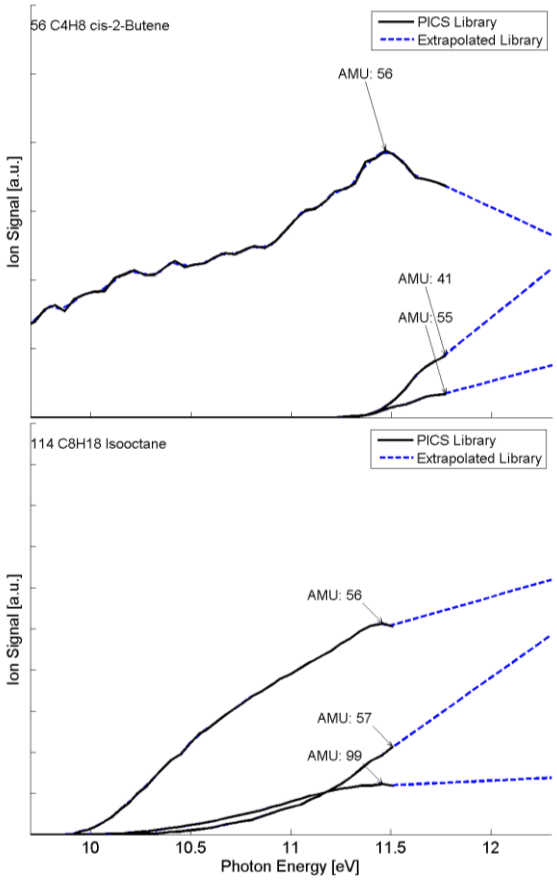

Figure 6. Plot of measured (solid black) and linearly extrapolated (dashed blue) photoionization cross-sections for cis-2-butene (top) and isooctane (bottom) across the range of photon energies examined here. Only ion fragments that produced greater than 1% of the total ion signal are plotted.

The term SW represents the total number of sweeps by the multichannel plate detector for each energy, which was fixed at half a million for each scan for the current experiments. Finally, the instrument-dependent proportionality constant C was determined from an analysis of the calibration gases described earlier and was on the order of 1 for the current experiments. Total measured signal is then the sum of signal contributions from each sample constituent (i.e., $S = \sum_i S_i$).

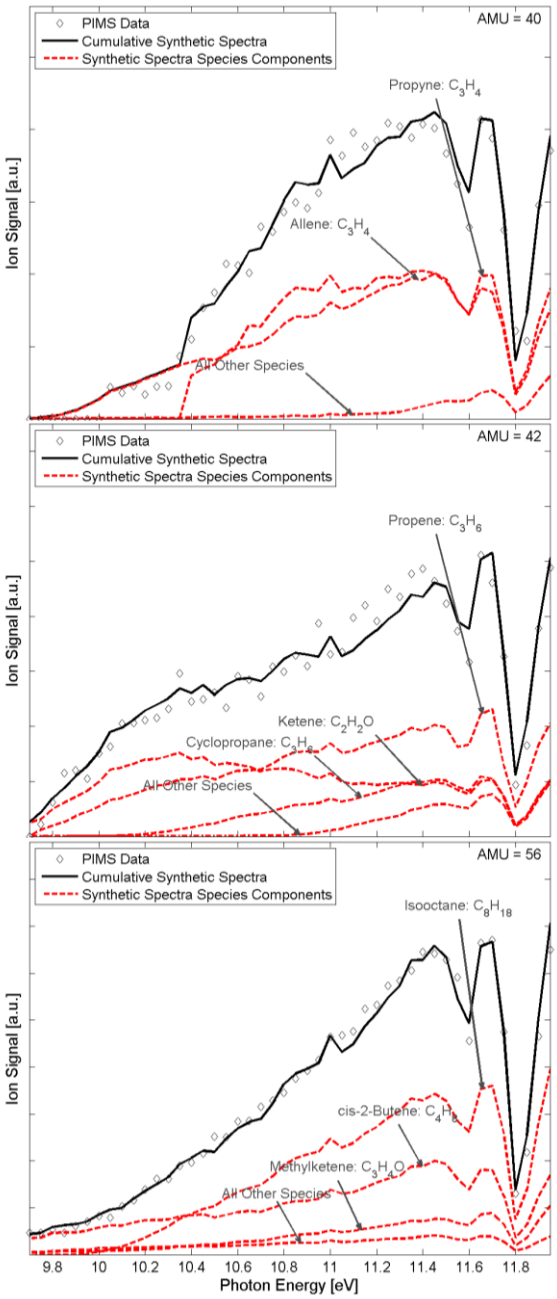

Figure 7. Photoionization efficiency curves for species sampled from the globally rich NVO operating condition (SOI = -40 CAD_{NVO}) at AMU values of 40, 42, and 56 compared to individual PIE curves for select species along with the cumulative synthetic signal.

To determine sample speciation from the energy scan image, photoionization libraries and measured calibration terms from eqn. 1 were used to create synthetic photoionization efficiency (PIE) curves for each species. Species PIE curves were summed to create a synthetic energy scan image, with species concentrations iteratively adjusted until the synthetic image intensity closely matched that of

the measured energy scan signal image. Since photoionization cross-section libraries for certain species are similar, it is possible that nearly identical synthetic signal images could be produced from various constituent combinations. Accordingly, select species were removed from the cross-section libraries if it was determined that their presence was unlikely and they complicated the analysis. A synthetic signal image is provided in the bottom of Figure 5that corresponds to the original energy scan image. As can be seen, the agreement with the raw energy scan image is very good

In Figure 7, the measured signal from the globally rich NVO operating condition (SOI = -40 CAD_{NVO}) is compared to the cumulative PIE curves for relevant species at select ion mass values. The signal at AMU 40 is best reproduced by a weighted sum of the reference PIE curves for allene and propyne, with minor contributions from several other species. Similarly, the signal at AMU 42 is mostly from propene, ketene, and cyclopropane. The signal at AMU 56 is dominated by the parent isooctane, with significant contributions from cis-2-butene and methylketene. In each case, the cumulative PIE curve is well matched to the measured signal. It is important to note that photoionization cross-sections could be much larger for the fragment ions than for the parent molecule; particularly for larger species such as isooctane.

Results and Discussion

Engine performance with fuel type

A goal of the current project is to compare sampling data analyzed via PIMS to earlier GC measurements for the lean NVO operating condition acquired from the same engine by Steeper and Davisson [22]. However, it is first necessary to confirm that NVO-cycle reactions and main-cycle combustion phasing were consistent. A comparison of NVO-cycle apparent heat release (AHR) data across a range of NVO SOI from both studies are plotted in Figure 8. The current results include data from the engine fueled separately by isooctane (circles) and RD587 gasoline (triangles) to examine the impact of fuel-type on performance characteristics.

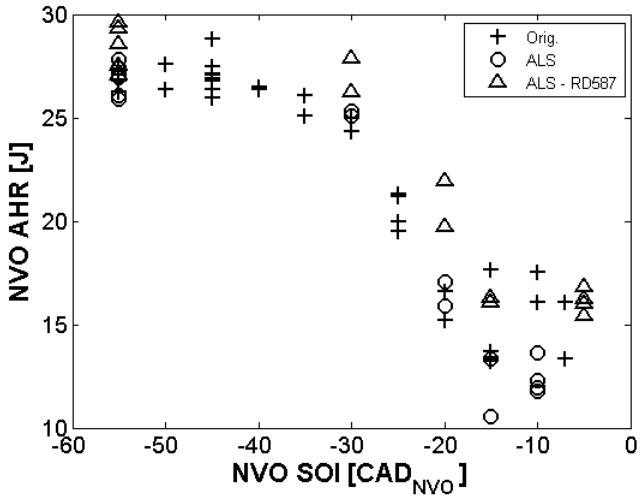

Figure 8. NVO cycle apparent heat release for the fuel-lean NVO cycle injection sweep with either isooctane (circle) or RD587 gasoline (triangle) fueling. Results are compared to earlier performance data with isooctane fueling (+).

For the current study at the earliest NVO SOI (-55 CAD_{NVO}), ~27 J of heat release were produced when the engine was fueled by isooctane. This value decreased slightly to ~25 J as the NVO SOI was retarded to -30 CAD_{NVO}, and dropped precipitously with additional NVO injection retard. In all instances, the apparent heat release was well-matched to previous experiments by Steeper and Davisson [22]. The heat release for the engine fueled by RD587 gasoline on the other hand was consistently 1-2 J higher across all NVO injection timings. Recall that while main-cycle fueling rates were adjusted to maintain constant fuel energy in the combined main and NVO cycles, the NVO fueling rates were fixed. Accordingly, the additional NVO-cycle heat release is attributed to the slightly larger unit energy per volume for the RD587 relative to isooctane. It is also possible that differences in chemical reactivity and mixing characteristics played a role.

The reduction in heat release with NVO SOI retard led to an associated decrease in main intake charge heating. Despite this fact, Figure 9 shows that main-cycle heat release CA10 (location of 10 % mass-burned point) advances with SOI retard. As previously noted [22], this trend is evidence of a chemical effect of NVO fueling from localized rich reaction zones that are believed to produce reactive species that carry over and enhance main combustion. As with the NVO heat release characteristics, the total main-cycle heat release was well matched with previous datasets regardless of fuel-type. Moreover, the CA10 across the sweep of NVO SOI was well-matched for the isooctane fueling. The RD587 fueling had a 1-2 CAD advance of CA10 relative to similar isooctane data, possibly due to the higher RD587 fuel reactivity.

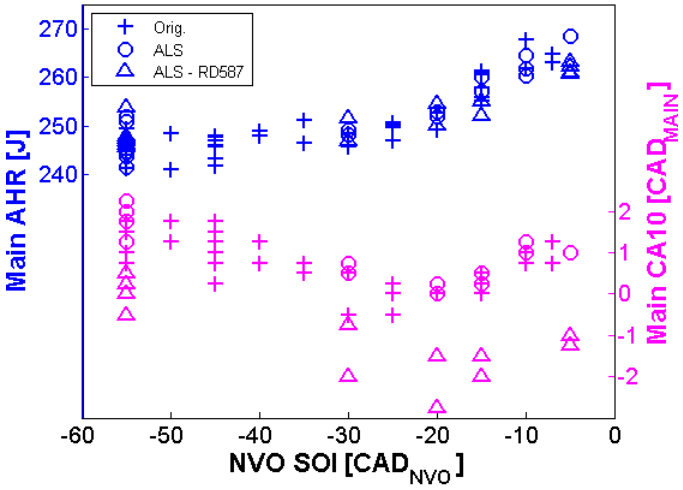

Figure 9. Main-cycle AHR and CA10 for the fuel-lean NVO cycle injection sweep with either isooctane (circle) or RD587 gasoline (triangle) fueling. Results are compared to earlier performance data with isooctane fueling (+).

Gas Sampling Results

Selected species, identified from the PIMS analysis, that appear in high concentrations are presented in the following sub-sections. These results are compared to previous GC measurements for the same condition. Note that methane, hydrogen, carbon monoxide, and carbon dioxide were not measured by the PIMS diagnostic since the highest energy scan level for the current experiments (12.3 eV) was below the photoionization potential for these species. Moreover, methanol was difficult to resolve since its dominant PIE signal overlapped that of oxygen, which appeared in large concentrations.

Fuel-Lean NVO Operation Sampling Results

Parent isooctane and isobutene speciation results for the fuel-lean NVO operating condition SOI sweep are shown in Figure 10 for the isooctane fueled condition. PIMS results are compared to GC measurements [22] acquired from the same engine with identical operating conditions and collection protocols. The PIMS isooctane measurement from the exhaust samples is also included for reference. It should be noted that little useful speciation information was obtained from the sample speciation of the NVO cycle fueled by the RD587 certification gasoline. Although poor SNR for the PIMS diagnostic played a role, the main challenge was the large number of fuel constituents with an even larger number of fuel intermediates that led to a high degree of intractable channel cross-talk. Furthermore, it is likely that the current suite of PICS libraries is insufficient for the complex mixture of hydrocarbon components present in the sample. Accordingly, only results for acetylene are reported here, as the species measurement appears to be free from bias. Finally, there is far too much data to plot here. Accordingly PIMS sampling results are tabulated in Appendix A for all SOI investigated.

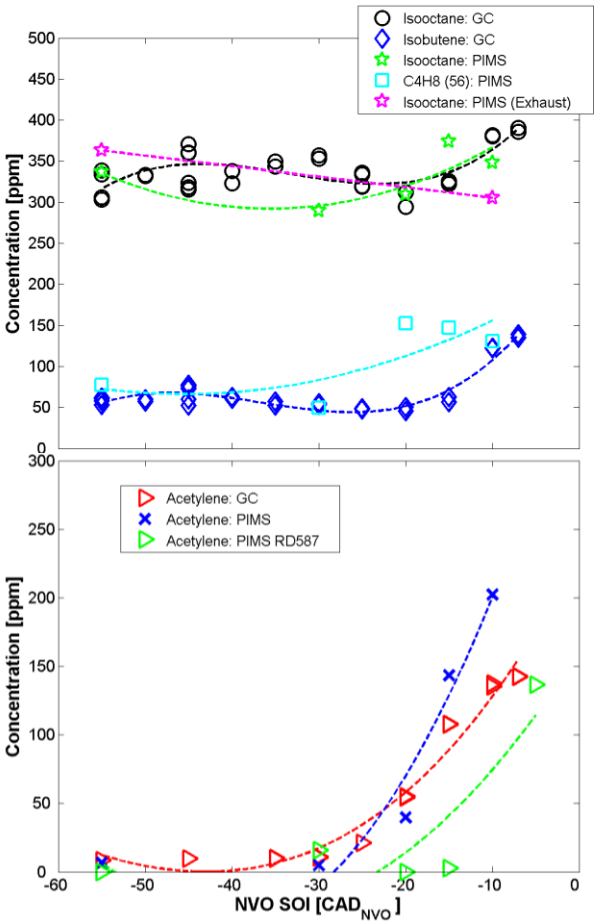

Figure 10. Top: Comparison of PIMS isooctane and butene isomer measurements to previous GC measurements [22] across a sweep of NVO injection timings for the globally lean NVO operating condition. Bottom: comparison acetylene PIMS and GC measurements, along with PIMS measured acetylene for the engine fueled by RD587 gasoline.

From the results in Figure 10, it is apparent that within the range of reproducibility, isooctane concentrations from both the GC and PIMS diagnostics are well matched across the range of NVO SOI. Moreover, while the data for isobutene (not shown) from the PIMS diagnostic are below the corresponding measured GC values, this is likely due to the fact that the GC uses isobutene as a proxy for the sum total of all butene isomers. When the PIMS-measured concentrations of these isomers are considered, the cumulative total is in good agreement with the GC data. Exhaust-sample isooctane concentrations were nearly equivalent to the corresponding NVO-cycle samples. Peterson et al. [24] attributed a large portion of these hydrocarbons to overly lean end-of-injection bulk-gas mixtures that are likely invariant to changes in NVO-cycle SOI.

For acetylene concentrations in the lower plot of Figure 10, the absolute agreement between the PIMS and earlier GC results was reasonably good. The worst agreement was with the more retarded SOI where PIMS measured acetylene concentrations were up to 35% greater than the corresponding GC measurement. The reason for the variation is not entirely clear, but the poor PIMS SNR already discussed played a role. It is also possible that channel cross-talk from hydrocarbon fragments was not sufficiently accounted for during post-processing. Nonetheless, trends were consistent with the previous measurements. Sample results from the engine fueled by RD587 are also included for comparison. Acetylene yields once again were well matched to the earlier GC datasets. The result suggests increased acetylene production from locally-rich pool fires produced from fuel spray impingement for retarded SOI was similarly responsible for the observed reactivity enhancement when the engine was fueled by RD587 gasoline.

Results for small (e.g., formaldehyde, ethanol, dimethyl-ether, and formic acid) and intermediate sized oxygenates (e.g., methylketene, allyl alcohol) are plotted in Figure 11. Species with similar PIE curves were lumped together since they could not be accurately characterized without better SNR. Speciation results for the smaller oxygenates were largely invariant across the range of SOI, and were similar to the exhaust recorded values. There was a minima for all smaller oxygenates at -30 CAD$_{NVO}$, that quickly rebounded to the original values with NVO SOI advance or retard. For the medium sized oxygenates, concentrations more than doubled as the NVO SOI was retarded from the earliest to the latest timings.

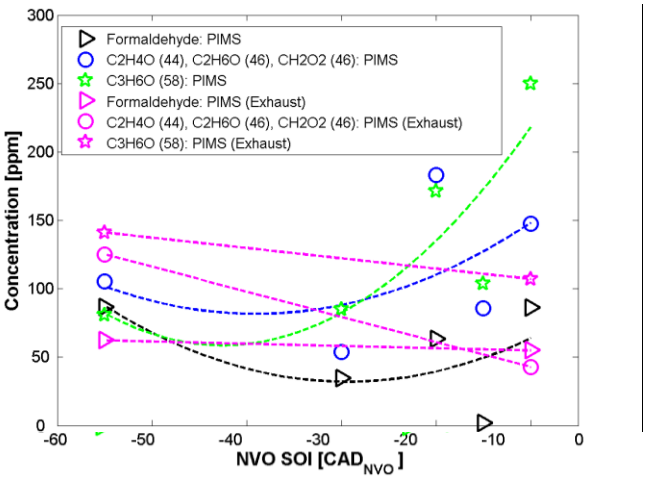

Figure 11. PIMS sampling data for the small (formaldehyde, ethanol, dimethyl-ether, and formic acid) and intermediate sized volatiles (allyl alcohol and methylketene), across the NVO sweep for the fuel-lean NVO operating condition. Due to poor SNR, similar species were summed together.

Fuel-Rich NVO Operation Sampling Results

As described in the Approach section, a fuel-rich NVO operating condition was similarly investigated. Due to the unique operating characteristics where the dump-cycle fueling rate was adjusted from the warm-up cycle value, there are no performance data for the operating condition. As with the lean operating condition, PIMS analyzed results are compared when available to previous GC data.

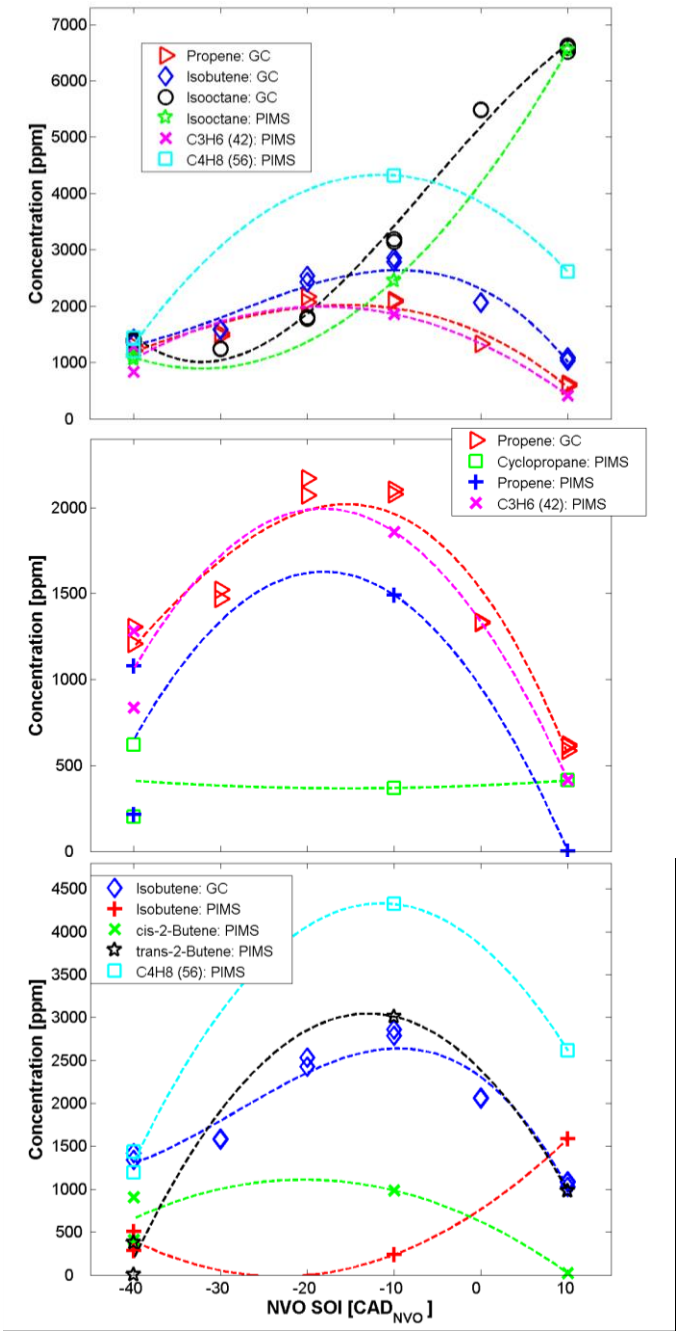

Figure 12. Top. Comparison of PIMS measured large hydrocarbon species to previous GC measurements [27] for the fuel-rich NVO SOI sweep. Middle: Comparison of PIMS measured propene isomers (C3H6) to previous GC measurements of propene. Bottom: Comparison of PIMS measured butene isomers (C4H8) to previous GC measurements of isobutene.

The top plot in Figure 12 compares PIMS measured yields of isooctane and the cumulative total for the propene (C3H6) and butene (C4H8) isomers to corresponding GC measurements from Szybist et al. [27]. The agreement to the GC data is excellent for the isooctane and the propene isomer species. The middle plot compares PIMS measured C3H6 species and reveals there is a constant cyclopropane baseline (~500 ppm) across the NVO SOI sweep, with the difference made up by propene. Trendwise agreement between PIMS and GC data for butene isomers is good, with peak values occurring at an NVO SOI of -10 CAD_{NVO} and tailing off with either NVO SOI advance or retard. However, the absolute agreement is fairly poor, as the PIMS values are roughly double the GC measurements. The breakdown in butene isomer constituents shows that the GC data agree well with the trans-2-butene concentrations, but the inclusion of cis-2-butene and isobutene concentrations lead to higher cumulative PIMS values. Note that significant propane quantities measured by earlier GC measurements were not observed with PIMS; future GC calibrations gases should be adjusted to reflect its absence.

Acetylene and ethylene concentrations are plotted in the top graph of Figure 12, with comparisons again made between the current PIMS measurements and the previous GC data. The FID column used to speciate the smaller hydrocarbons had too fast of an elution time, with the acetylene and ethylene co-eluting. Thus, only the cumulative total is reported here. Nonetheless, the agreement between the cumulative acetylene and ethylene measurements from the PIMS data is once again nearly exact to the GC measurements.

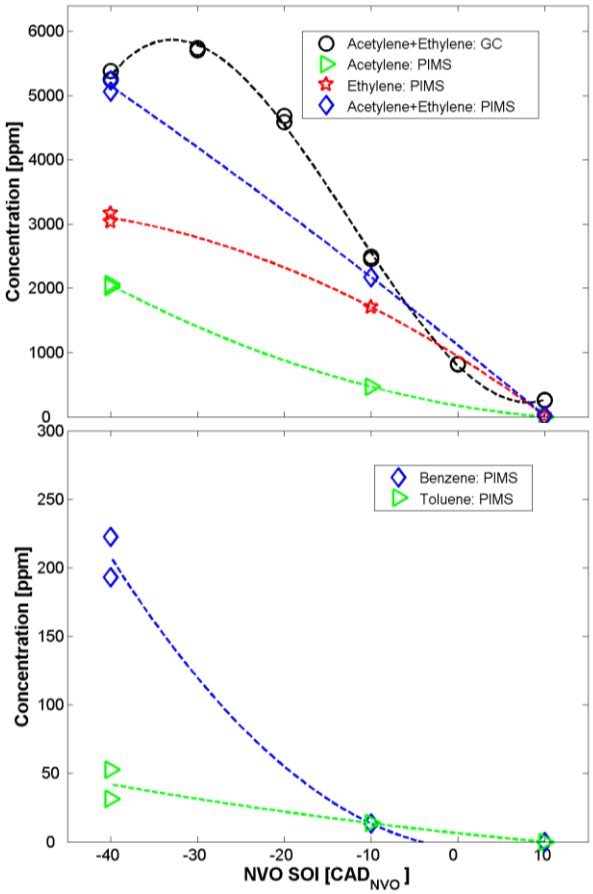

Figure 13. Comparison of PIMS measured acetylene and ethylene hydrocarbon species to previous GC measurements [27] for the fuel-rich NVO SOI sweep. Bottom: PIMS measured benzene and toluene concentrations.

Finally, PIMS results for the simple aromatics, benzene and toluene are graphed in the bottom plot of Figure 13. Although concentrations are small, the behavior closely mirrors that for the C_2 hydrocarbons as the yields are very low at the latest NVO SOI, and rapidly increase with NVO SOI advance. Peterson et al. [24] noted that for these oxygen deficient environments, the increased residence time from earlier NVO-cycle fuel injection enables additional time for slow pyrolysis reactions to convert excess fuel carbon into these soot precursors. Presently most detailed combustion chemistry kinetics mechanisms only consider molecular decomposition processes, and are not designed to account for the growth of polycyclic aromatic hydrocarbons (PAHs). These data indicate that PAH growth processes are an important detail that is necessary to better understand NVO-cycle reactions for oxygen-deficient environments.

Summary and Conclusions

Gas sampling and speciation of NVO end-cycle products was performed using a custom dump-valve system in a single-cylinder research engine operating under low-load LTGC. Samples were collected by a custom dump-valve apparatus with the engine fueled by either isooctane or an 88-octane research certification gasoline. Fuel-lean and fuel-rich NVO operating conditions under a sweep of NVO injection timings were selected as these matched previous studies with speciation via GC diagnostics. Detailed gas composition measurements were achieved via photoionization mass spectroscopy using synchrotron generated vacuum-ultraviolet light and a Sandia owned flame sampling apparatus located at the Lawrence Berkeley National Laboratory Advanced Light Source. Custom post-processing algorithms were developed to analyze collected energy scan data that used detailed photoionization cross-section libraries. This work represents the first-ever application of PIMS to quantify collected engine samples. Major findings are as follows:

- NVO sample speciation data obtained via PIMS agreed very well with previous GC measurements for nearly all species examined, despite the complex mixture of sampled species with significant amounts of signal cross-talk. However, definitive speciation could not be achieved from the NVO engine samples with RD587 gasoline fueling. This was in part due to poor SNR, but was mostly a result of the complex mix of gasoline constituents that led to a high degree of intractable channel cross-talk.

- For fuel-lean NVO operation, the NVO and main cycle heat release characteristics for isooctane and RD587 gasoline fueling were nearly identical if the total amount of fuel energy injected was fixed. The only differences of note with RD587 gasoline fueling are increased NVO-cycle apparent heat release (~1-2 J) and advanced main-cycle CA10 (~1-2 CAD). Both effects were attributed to enhanced gasoline reactivity.

- Acetylene was measured by the PIMS diagnostic for the RD587 gasoline fueling, with measured values that agreed well with corresponding values from the engine fueled by isooctane.

- For fuel-lean NVO operation, significant volatile species quantities were measured by the PIMS diagnostic. For most of these species, NVO-cycle measurements were roughly equivalent to measured exhaust concentrations. The exception was for the larger oxygenates (e.g., allyl alcohol and methylketene), which exhibited a strong increase with NVO SOI retard.

- For fuel-rich NVO operation, the cumulative concentrations of intermediate isomers for the most part agreed well with earlier single-component measurements by the GC. However, dominant isomers often differed from earlier GC calibrations.

- Steadily increasing concentrations of benzene and toluene with NVO SOI advance were observed for the fuel-rich NVO condition. The trends are well matched to those previously observed for acetylene, with increases attributed to longer residence times needed for fuel pyrolysis. This is an important finding since available detailed kinetics mechanisms for isooctane combustion do not predict this behavior.

PIMS data will be used to update the palate of calibration gases for the in-house GC diagnostic. Furthermore, the tabulated results in the appendix can serve as validation benchmarks for future detailed chemistry and multidimensional modeling efforts. Future work will involve similar testing using different representative gasoline fuel components (e.g., aromatics, napthas, ethanol), with a focus on fuel-rich oxygen environments. A series of modifications to the flame sampling diagnostic will be performed to increase SNR by an order of magnitude to hopefully more clearly identify species with similar photoionization cross-section characteristics.

References

1. Caton JA, "Thermodynamic Advantages of Low Temperature Combustion (LTC) Engines Using Low Heat Rejection (LHR) Concepts," SAE Technical Paper 2011-01-0312, 2011, doi: 10.4271/2011-01-0312.
2. Sjöberg M, Dec JE, "An Investigation into Lowest Acceptable Combustion Temperatures for Hydrocarbon Fuels in HCCI Engines," *P. Combust. Inst.*, 30:2719-26, 2005, doi: 10.1016/j.proci.2004.08.132.
3. Wermuth N, Yun H, Najt P, "Enhancing Light Load HCCI Combustion in a Direct Injection Gasoline Engine by Fuel Reforming During Recompresion," *SAE Int. J. Engines*, 2 (1):823-36, 2009, doi: 10.4271/2009-01-0923.
4. Weall A, Szybist JP, Edwards KD, Foster M, Confer K, Moore W, "HCCI Load Expansion Opportunities Using a Fully Variable HVA Research Engine to Guide Development of a Production Intent Cam-Based VVA Engine: The Low Load Limit," SAE Technical Paper 2012-01-1134, 2012, doi: 10.4271/2012-01-1134.
5. Zhao H, Peng Z, Williams J, Ladommatos N, "Understanding the Effects of Recycled Burnt Gases on the Controlled Autoignition (CAI) Combustion in Four-Stroke Gasoline Engines," SAE Technical Paper 2001-01-3607, 2001, doi: 10.4271/2001-01-3607.
6. Onishi S, Jo SH, Shoda K, Jo PD, Kato S, "Active Thermo-Atmosphere Combustion (ATAC) - A New Process for Internal Combustion Engines," SAE Technical Paper 790501, 1979, doi: 10.4271/790501.
7. Noguchi M, Tanaka Y, Tanaka T, Takeuchi Y, "A Study on Gasoline Engine Combustion by Observation of Intermediate Reactive Products during Combustion," SAE Technical Paper 790840, 1979, doi: 10.4271/790840.
8. Koopmans L, Denbratt I, "A Four Stroke Camless Engine, Operated in Homogeneous Charge Compression Ignition

Mode with Commercial Gasoline," SAE Technical Paper 2001-01-3610, 2001, doi: 10.4271/2001-01-3610.
9. Urushihara T, Hiraya K, Kakuho A, Itoh T, "Expansion of HCCI Operating Region by the Combination of Direct Fuel Injection, Negative Valve Overlap and Internal Fuel Reformation," SAE Technical Paper 2003-01-0749, 2003, doi: 10.4271/2003-01-0749.
10. Koopmans L, Ogink R, Denbratt I, "Direct Gasoline Injection in the Negative Valve Overlap of a Homogeneous Charge Compression Ignition Engine," SAE Technical Paper 2003-01-1854, 2003, doi: 10.4271/2003-01-1854.
11. Waldman J, Nitz D, Aroonsrisopon T, Foster D, Iida M, "Experimental Investigation into the Effects of Direct Fuel Injection During the Negative Valve Overlap Period in a Gasoline Fueled HCCI Engine," SAE Technical Paper 2007-01-0219, 2007, doi: 10.4271/2007-01-0219.
12. Aroonsrisopon T, Nitz DG, Waldman JO, Foster DE, Iida M, "A Computational Analysis of Direct Fuel Injection During the Negative Valve Overlap Period in an Iso-Octane Fueled HCCI Engine," SAE Technical Paper 2007-01-0227, 2007, doi: 10.4271/2007-01-0227.
13. Berntsson AW, Denbratt I, "Optical study of HCCI Combustion using NVO and an SI Stratified Charge," SAE Technical Paper 2007-24-0012, 2007, doi: 10.4271/2007-24-0012.
14. Berntsson AW, Andersson M, Dahl D, Denbratt I, "A LIF-study of OH in the Negative Valve Overlap of a Spark-assisted HCCI Combustion Engine," SAE Technical Paper 2008-01-0037, 2008, doi: 10.4271/2008-01-0037.
15. Song HH, Edwards CF, "Optimization of Recompression Reaction for Low-Load Operation of Residual-Effected HCCI," SAE Technical Paper 2008-01-0016, 2008, doi: 10.4271/2008-01-0016.
16. Rothamer DA, Snyder JA, Hanson RK, Steeper RR, Fitzgerald RP, "Simultaneous imaging of exhaust gas residuals and temperature during HCCI combustion," *P. Combust. Inst.*, 32:2869-76, 2009, doi: 10.1016/j.proci.2008.07.018.
17. Fitzgerald RP, Steeper R, "Thermal and Chemical Effects of NVO Fuel Injection on HCCI Combustion," *SAE Int. J. Engines*, 3 (1):46-64, 2010, doi: 10.4271/2010-01-0164.
18. Fitzgerald RP, Steeper R, Snyder J, Hanson R, Hessel R, "Determination of Cycle Temperatures and Residual Gas Fraction for HCCI Negative Valve Overlap Operation," *SAE Int. J. Engines*, 3 (1):124-41, 2010, doi: 10.4271/2010-01-0343.
19. Zuehl JR, Ghandhi J, Hagen C, Cannella W, "Fuel Effects on HCCI Combustion Using Negative Valve Overlap," SAE Technical Paper 2010-01-0161, 2010, doi: 10.4271/2010-01-0161.
20. Borgqvist P, Tunestål P, Johansson B, "Investigation and Comparison of Residual Gas Enhanced HCCI using Trapping (NVO HCCI) or Rebreathing of Residual Gases," SAE Technical Paper 2011-01-1772, 2011, doi: 10.4271/2011-01-1772.
21. Hunicz J, "An Experimental Study of Combustion Phasing Control in CAI Gasoline Engine with In-Cylinder Fuel Reforming," SAE Technical Paper 2011-24-0052, 2011, doi: 10.4271/2011-24-0052
22. Steeper RR, Davisson ML, "Analysis of Gasoline Negative-Valve-Overlap Fueling via Dump Sampling," *SAE Int. J. Engines*, 7 (2):762-71, 2014, doi: 10.4271/2014-01-1273.
23. Puranam SV, Steeper R, "The Effect of Acetylene on Iso-octane Combustion in an HCCI Engine with NVO," *SAE Int. J. Engines*, 5 (4):1551-60, 2012, doi: 10.4271/2012-01-1574.
24. Peterson B, Ekoto I, Northrop W, "Investigation of Negative Valve Overlap Reforming Products Using Gas Sampling and Single-Zone Modeling," *SAE Int. J. Engines*, 8 (2):747-57, 2015, doi: 10.4271/2015-01-0818.
25. Snyder JA, Hanson RK, Fitzgerald RP, Steeper RR, "Dual-Wavelength PLIF Measurements of Temperature and Composition in an Optical HCCI Engine with Negative Valve Overlap," *SAE Int. J. Engines*, 2 (1):460-74, 2009, doi: 10.4271/2009-01-0661.
26. Fitzgerald RP, Steeper RR, "Application of a Tunable-Diode-Laser Absorption Diagnostic for CO Measurements in an Automotive HCCI Engine," *SAE Int. J. Engines*, 3 (2):396-407, 2010, doi: 10.4271/2010-01-2254.
27. Szybist JP, Steeper RR, Splitter D, Kalaskar VB, Pihl J, Daw C, "Negative Valve Overlap Reforming Chemistry in Low-Oxygen Environments," *SAE Int. J. Engines*, 7 (1):418-33, 2014, doi: 10.4271/2014-01-1188.
28. Huelser T, Schulz C, Brands T, Grunefeld G, Koss H-J, Morcinkowski B, et al., "Probing Species Formed by Pilot Injection During Re-Compression in a Controlled Auto-Ignition Engine by H2CO LIF and Chemiluminescence Imaging," *SAE Int. J. Engines*, 7 (2):772-89, 2014, doi: 10.4271/2014-01-1275.
29. Peterson B, Baum E, Bohm B, Sick V, Dreizler A, "Evaluation of toluene LIF thermometry detection strategies applied in an internal combustion engine," *Appl. Phys. B*, 117 (1):151-75, 2014, doi: 10.1007/s00340-014-5815-0.
30. Arning J, Ramsander T, Collings N, "Analysis of In-Cylinder Hydrocarbons in a Multi-Cylinder Gasoline HCCI Engine Using Gas Chromatography," *SAE Int. J. Engines*, 2 (2):141-9, 2009, doi: 10.4271/2009-01-2698.
31. Yu W, Xie H, Chen T, Li L, Song K, Zhao H, "Effects of Active Species in Residual Gas on Auto-Ignition in a HCCI Gasoline Engine," SAE Technical Paper 2012-01-1115, 2012, doi: 10.4271/2012-01-1115.
32. Hunicz J, "An experimental study of negative valve overlap injection effects and their impact on combustion in a gasoline HCCI engine," *Fuel*, 117, Part A (0):236-50, 2014, doi: http://dx.doi.org/10.1016/j.fuel.2013.09.079.
33. Hessel RP, Steeper R, Fitzgerald R, Aceves S, Flowers D, "Full Cycle CFD Simulations to Study Thermal and Chemical Effects of Fuel Injection during Negative Valve Overlap in an Automotive Research Engine," SAE Technical Paper 2010-01-2236, 2010, doi: 10.4271/2010-01-2236.
34. Cool TA, McIlroy A, Qi F, Westmoreland PR, Poisson L, Peterka DS, et al., "Photoionization mass spectrometer for studies of flame chemistry with a synchrotron light source," *Review of Scientific Instruments*, 76 (9) 2005, doi: 10.1063/1.2010307.
35. Hansen N, Cool TA, Westmoreland PR, Kohse-Hoinghaus K, "Recent contributions of flame-sampling molecular-beam mass spectrometry to a fundamental understanding of combustion chemistry," *Prog Energ Combust*, 35 (2):168-91, 2009, doi: 10.1016/j.pecs.2008.10.001.

Contact Information: Isaac W. Ekoto, iekoto@sandia.gov, Sandia National Laboratories, MS 9053, PO Box 969, Livermore, CA 94551-0969, USA.

Acknowledgments

Research at Sandia was supported by the U.S. Department of Energy, Office of Vehicle Technologies. Sandia is a multiprogram laboratory operated by Sandia Corporation, a Lockheed Martin Company, for the United States Department of Energy's National Nuclear Security Administration under contract DE-AC04-94AL85000. We gratefully acknowledge insightful technical discussions with James Szybist at Oak Ridge National Laboratory and General Motors Research staff. We further acknowledge the engineering support provided by Alberto Garcia, which kept all aspects of the experiment operational.

Appendix A – Tabulated PIMS Speciation Data of NVO Samples

Table A1. Fuel-lean NVO sample PIMS measurements for all species recorded in significant quantities at each NVO SOI. All results are presented in molar concentration (ppm).

SOI [CAD_{NVO}]	C2H2 Acetylene	C2H4 Ethylene	C2H6 Ethane	CH2O Formaldehyde	C3H4 Allene
-55	7	58	10	86	27
-30	5	2	19	35	6
-20	40	17	44	63	14
-15	144	143	58	2	45
-10	202	164	133	86	7
SOI [CAD_{NVO}]	C3H4 Propyne	C3H5 2-Propenyl	C3H5 Allyl-radical	C3H6 Cyclopropane	C2H2O Ketene
-55	1	11	14	9	5
-30	1	0	0	0	21
-20	11	5	54	2	22
-15	0	86	26	2	1
-10	30	68	36	75	29
SOI [CAD_{NVO}]	C3H6 Propene	C2H6O Dimethyl-ether	C2H6O Ethanol	CH2O2 Formic-acid	C4H8 1-Butene
-55	61	0	80	26	6
-30	1	28	0	26	0
-20	27	33	51	99	6
-15	43	15	36	35	14
-10	39	22	104	22	73
SOI [CAD_{NVO}]	C4H8 Isobutene	C3H4O Methylketene	C4H8 cis-2-butene	C4H8 trans-2-butene	C3H6O 2-Propen-1-ol
-55	33	75	38	0	15
-30	17	99	14	18	0
-20	52	45	21	74	70
-15	22	50	0	111	59
-10	18	110	6	33	82
SOI [CAD_{NVO}]	C4H10 Isobutane	C3H6O Propen-2-ol	C3H6O Propylene-oxide	C3H6O Allyl-alcohol	C3H8O 2-Propanol
-55	2	1	14	50	29
-30	16	0	1	80	64
-20	20	31	27	21	0
-15	13	0	1	30	16
-10	18	24	52	76	45
SOI [CAD_{NVO}]	C2H4O2 Methyl-formate	C7H4 1-3-5-Heptatriyne	C4H8O2 Methyl-propanoate	C5H8O2 Ethyl-propenoate	C8H18 Isooctane
-55	0	22	13	0	336
-30	0	3	18	32	289
-20	216	41	25	0	310
-15	268	21	22	10	374
-10	255	30	16	32	348

Table A2. Fuel-rich NVO sample PIMS measurements for all species recorded in significant quantities at each NVO SOI. Note that the repeat values for -40 CAD_{NVO} are reported here. In some cases the agreement was very good, while at other times the values were not well reproduced. All results are presented in molar concentration (ppm).

SOI [CAD_{NVO}]	C2H2 Acetylene	C2H4 Ethylene	C2H6 Ethane	CH2O Formaldehyde	C3H4 Allene
-40	2025	3038	1	533	265
-40 (repeat)	2069	3163	304	743	190
-10	466	1707	250	933	689
10	0	17	1100	364	158
SOI [CAD_{NVO}]	C3H4 Propyne	C3H5 2-Propenyl	C3H6 Cyclopropane	C2H2O Ketene	C3H6 Propene
-40	293	0	202	161	1080
-40 (repeat)	367	2	620	454	216
-10	1	129	368	336	1490
10	30	601	413	117	1
SOI [CAD_{NVO}]	C2H4O Ethenol	C4H6 1-2-Butadiene	C4H6 1-3-Butadiene	C4H8 1-Butene	C4H8 Isobutene
-40	6	41	12	1	288
-40 (repeat)	10	1	110	143	508
-10	163	126	33	92	236
10	0	0	0	33	1585
SOI [CAD_{NVO}]	C3H4O Methylketene	C4H8 cis-2-butene	C4H8 trans-2-butene	C3H6O 2-Propen-1-ol	C3H6O Allyl-alcohol
-40	303	904	3	403	15
-40 (repeat)	243	409	374	1	360
-10	369	983	3010	179	611
10	798	21	978	1138	458
SOI [CAD_{NVO}]	C6H6 Benzene	C5H8O trans-2-Pentenal	C7H8 Toluene	C5H8O2 Ethyl-propenoate	C8H18 Isooctane
-40	222	60	31	135	1111
-40 (repeat)	193	1	14	122	1064
-10	13	286	0	323	2458
10	0	14	53	0	6545

Definitions/Abbreviations

AHR/AHRR	Apparent heat release/rate
ALS	Advanced Light Source
AMU	Atomic mass unit
CA10	Location of 10% mass-burned point
CAD	Crank angle degree
CAD_{MAIN}	CAD after main-cycle TDC
CAD_{NVO}	CAD after NVO-cycle TDC
COV	Coefficient of variation
DME	Dimethyl ether
EVC/EVO	Exhaust valve close / open
FID	Flame ionization detector
FTIR	Fourier transform infrared spectroscopy
GC	Gas chromatograph
IVC/IVO	Intake valve close / open
LBNL	Lawrence Berkeley National Laboratory
LLNL	Lawrence Livermore National Laboratory
LTGC	Low-temperature gasoline combustion
NVO	Negative valve overlap
OEM	Original equipment manufacturers
PAH	Polycyclic aromatic hydrocarbon
PICS	Photoionization Cross-Section
PID	Proportional-integral-derivative
PIMS	Photoionization Mass Spectroscopy
ppm	parts per million
rpm	Revolutions per minute
SOI	Start of injection
SNR	Signal to noise
TCD	Thermal conductivity detector
TDC_{NVO}	Top dead center for the NVO cycle
TDC	Top dead center
VUV	Vacuum Ultraviolet